Optimizing Interface Conductivity in Electronics

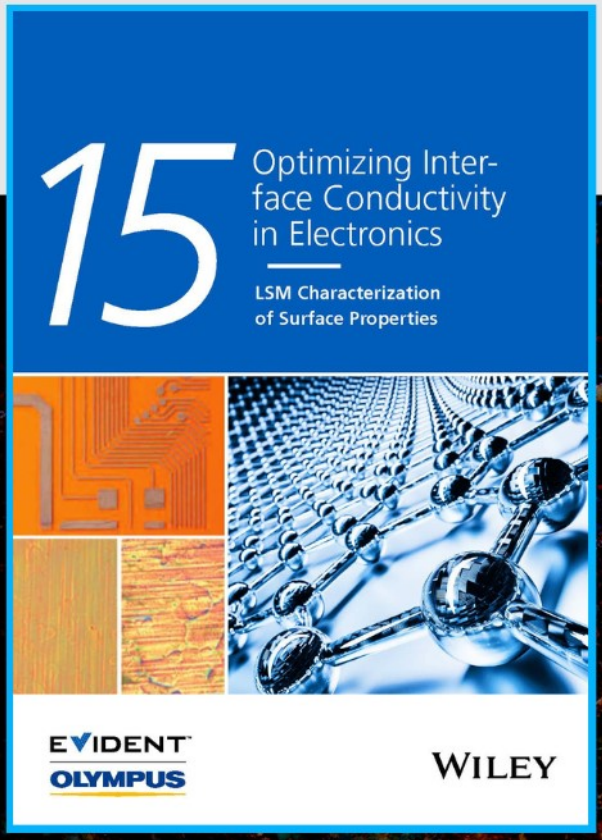

The latest eBook from Advanced Optical Metrology. Download for free.

Surface roughness is a key parameter for judging the performance of a given material's surface quality for its electronic application. A powerful tool to measure surface roughness is 3D laser scanning confocal microscopy (LSM), which will allow you to assess roughness and compare production and finishing methods, and improve these methods based on mathematical models.

Focus on creating high-conductivity electronic devices with minimal power loss using laser scanning microscopy is an effective tool to discern a variety of roughness parameters.

EVIDENT
OLYMPUS

WILEY

Check for updates

ADVANCED ELECTRONIC MATERIALS
www.advelectronicmat.de

Enhancement of Interfacial Polarization in $BaTiO_3$ Thin Films via Oxygen Inhomogeneity

Zhipeng Li, Zeyu Zhang, Jia Liu, Ruixue Zhu, Binghui Ge,* Yueliang Li, Xin Zhang, Peng Gao, Dawei Wang, Xiaoguang Xu, Wenhuai Tian, and Yong Jiang**

Enhancement of interfacial ferroelectricity is crucial for the development of nanoscale ferroelectric devices, such high density and nonvolatile memory. Although the epitaxial strain can lead to improved properties, the limited choices of substrates and strain relaxation have hindered the further tuning of ferroelectricity by strain engineering. To overcome this limitation, the interaction between polarization and defects is regarded as a potential route to enhance the interfacial polarization. Here, a universal method to achieve a polarization-enhanced interface by tuning the distribution of oxygen in lead-free $BaTiO_3$ films is demonstrated. The interfacial phase processes largely increased *c*-axis lattice constant, tetragonality, and about 100% increasement of Ti atom displacement near interface within thickness of 8 unit cells, suggesting enhancement of spontaneous polarization up to 70 μC cm^{-2}. The gradient distribution of oxygen along *c*-axis is also revealed. In addition, the first-principle Monte Carlo simulation of the tetragonality and polarization support the experimental results. It is suggested that the inhomogeneity of oxygen and interfacial charges could induce an electric field and further enhance the interfacial polarization. This work provides a new route of utilizing the oxygen distribution to engineer the ferroelectrics and paves the way for the development of nanoscale ferroelectric devices.

1. Introduction

The advancement of thin-film growth technology enables us to modify and optimize functional properties including electronic, magnetic, and optical properties.[1,2] Particularly in ferroelectric materials, the substrate-induced epitaxial strain can lead to lattice deformation and enhance the ferroelectric properties, for instance, the enhanced ferroelectric transition temperature of $BaTiO_3$ (BTO) and room temperature ferroelectricty of $SrTiO_3$(STO).[3] However, the strain engineering is basically hampered due to limited commercially single crystal substrates and film-thickness-driven strain relaxation. Another tuning strategy is defects control. The defects, including point defects and extended defects sometimes unavoidable even in well-controlled growth conditions. They are usually detrimental to ferroelectricity, such as the increase of leakage current induced by oxygen vacancies, as well as the decrease of local spontaneous polarization near the defects.[4,5] However, defects can also be used to enhance the ferroelectric properties in some well-controlled conditions.[6] It was reported that the distortion due to coupling between strain and point cation defect complexes (so-called defect dipole) alignment could be associated with enhancement of ferroelectric Curie temperature and some other properties change.[7,8] From the aspect of oxygen vacancies, Liu et al. found that the

Z. Li, Z. Zhang, X. Zhang, X. Xu, W. Tian, Y. Jiang
School of Materials Science and Engineering
University of Science and Technology Beijing
Beijing 100083, China
E-mail: zplmse@ustb.edu.cn; yjiang@ustb.edu.cn

J. Liu, D. Wang
The School of Microelectronics and State Key Laboratory for Mechanical Behavior of Materials
Xi'an Jiaotong University
Xi'an 710049, China

R. Zhu, P. Gao
International Center for Quantum Materials
Electron Microscopy Laboratory
School of Physics
Peking University
Beijing 100871, China

B. Ge
Information Materials and Intelligent Sensing Laboratory of Anhui Province
Key Laboratory of Structure and Functional Regulation of Hybrid Materials of Ministry of Education
Institutes of Physical Science and Information Technology
Anhui University
Hefei 230601, China
E-mail: bhge@ahu.edu.cn

Y. Li
Central Facility of Electron Microscopy
Electron Microscopy Group of Materials Science
Ulm University
Albert-Einstein-Allee 11, 89081 Ulm, Germany

The ORCID identification number(s) for the author(s) of this article can be found under https://doi.org/10.1002/aelm.202100876.

DOI: 10.1002/aelm.202100876

 © 2021 Wiley-VCH GmbH

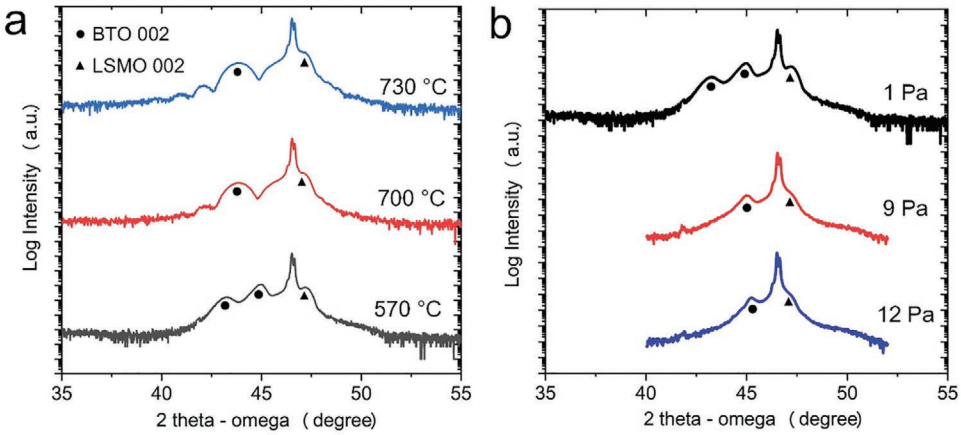

Figure 1. a) The XRD patterns of BTO/LSMO films on $SrTiO_3$ (001) substrate, growing under different substrate temperatures (570, 700, and 730 °C). b) Samples grown under different oxygen pressure (1, 9, and 12Pa) with a substrate temperature of 570 °C.

chemical valence and polarization discontinuity in the $PbTiO_3$/$BiFeO_3$ (PTO/BFO) heterostructures could induce accumulation of oxygen vacancies at the interface, where the interfacial polarization could be enhanced. Although oxygen vacancy has potential in the enhancing local polarization of ultrathin films, the effect exists in only ≈0.4–0.8 nm (≈1–2 unit cells),[9,10] which is far less than the required barrier layer thickness (3–5 nm) for the application of ferroelectric devices, such as ferroelectric tunnel junction.[11] Therefore, the active control of oxygen vacancies distribution to further enhance the ferroelectricity on a large scale is still an open question.

One of the mechanisms for determining the distribution of defects in ferroelectrics is the coupling between spontaneous polarization and charged defects.[12,13,14] The ferroelectric polarization could drive charged defects (e.g., oxygen vacancies) to migrate towards the energetically favorite sites, resulting in some defect complexes. Normally, the intrinsic polarization which can tune the defects formation is the internal electric field (E_{int}).[15] Its magnitude is determined by various sources, mainly interfacial charge discontinuity (E_{if}, internal electric field contributed by interfacial charge)[16,17] and strain gradient (E_{flexo}, internal electric field due to strain gradient generated flexoelectric effect).[18–21] It had been shown that the flexoelectricity, as well as the internal electric field, could be well controlled by thin-film growth temperatures, therefore, the interaction between oxygen vacancies could be modulated by various internal electric fields which is dependent on the growth temperature.[13] In this study, we tailored the distribution of oxygen through the internal electric field (by growth condition control) to enhance the interfacial polarization in BTO epitaxial films. The growth temperature and oxygen pressure were used to modulate the strain gradient and oxygen content, respectively. Aberration corrected transmission electron microscopy (TEM) imaging, as well as quantitative analysis, was used to characterize the lattice spacing, tetragonality, and polarization. The scanning TEM (STEM) and electron energy loss spectroscopy (EELS) analysis were used to analyze the local chemical composition. In addition, theoretical simulation was also conducted. It is demonstrated that largely enhanced local polarization (within ≈3nm) and structural phase separation can be induced via the active control of oxygen inhomogeneity. It should be noted that the polarization enhancement mechanism is not as same as the one reported in the literature which uses oxygen vacancies themselves to enlarge the unit cell volumes and tetragonality. Here we use the gradient of oxygen content to achieve the interfacial area (lower concentration of oxygen vacancies) sandwiched by oxygen vacancies with positive charges in the upper region and interfacial negative charges, which could form an artificial electric field and further enhance the polarization. This study offers a new approach to improve the interfacial polarization through oxygen.

2. Results and Discussion

Systematic growth of BTO films (60 nm) was conducted on $SrTiO_3$ (STO) (001) single crystal substrates via pulsed laser deposition (PLD). 20 nm thick LSMO serves as a bottom electrode of the ferroelectric film. The surface of the substrate was processed by heat and chemical treatment to achieve TiO_2 termination. The strain relaxation and introduction of oxygen vacancies are controlled by growth temperature and oxygen partial pressure during laser ablation process, respectively. **Figure 1**a shows the X-ray diffraction patterns, demonstrating the change in c-axis lattice parameters of samples. The BTO films grown under substrate temperatures of 730, 700, and 570 °C with an oxygen pressure of 1 Pa, referred to as BT (I), BT (II), and BT (III), respectively. It is revealed that the *c*-axis lattice parameter of BT (I) and BT (II) is 0.411 nm. By contrast, BT (III) has two sets of *c*-axis lattice plane reflections corresponding to 0.418 and 0.403 nm, suggesting possible structural phase separation. The BTO films grown at 570 °C with increased oxygen pressures (9 and 12 Pa) are 0.403 and 0.402 nm, respectively, Supporting Information, and no BTO diffraction peak splitting can be observed, which indicates the oxygen vacancies may contribute to the possible phase separation. The selected area electron diffraction (SAED) was also carried out, as shown in Figure S1, Supporting Information. It is shown that the film was epitaxially grown with single crystallinity. Reciprocal space mapping in Figure S2, Supporting Information, could confirm that there

© 2021 Wiley-VCH GmbH

2199160x, 2022, 2, Downloaded from https://onlinelibrary.wiley.com/doi/10.1002/aelm.202100876 by Peking University Health, Wiley Online Library on [04/09/2023]. See the Terms and Conditions (https://onlinelibrary.wiley.com/terms-and-conditions) on Wiley Online Library for rules of use; OA articles are governed by the applicable Creative Commons License

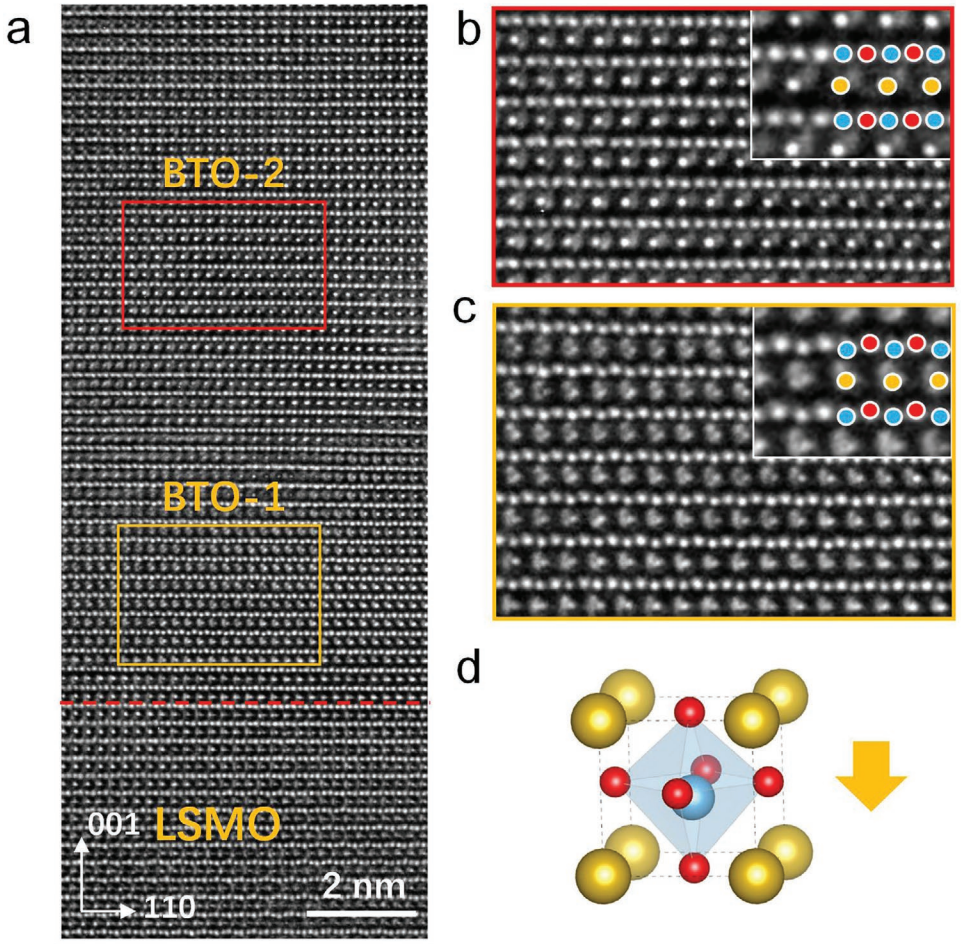

Figure 2. a) The negative spherical aberration-corrected TEM images of BTO/LSMO heterostructures. b,c) The enlarged images of BTO-2 and BTO-1 marked in a). The position of Ba (yellow), Ti (blue), and O (red) atoms are marked. d) The crystal structure of BTO unit cells near BTO/LSMO interface with polarization downwards. The TEM image simulation could be found in Figures S3 and S4, Supporting Information.

are two phases in BTO films (grown at 570 °C and oxygen pressure of 1Pa).

The large expansion of the *c*-axis lattice parameter observed by X-ray diffraction (0.418 nm) is normally associated with a large polarization in BT(III). To gain further insight into the lattice parameter, structural phase separation, and polarization, spherical aberration-corrected TEM analysis was conducted. **Figure 2**a shows an image of an interfacial area between LSMO and the *c*-axis oriented BTO. The image is recorded with an electron beam parallel to the [110] direction by the negative spherical aberration imaging (NCSI) condition.[22] Under this imaging condition, the atoms give negative phase contrast and appear bright on a dark background, possessing a high signal-to-noise ratio for quantitative measurement of cations (Ba and Ti) and anions (O) positions, with the additional advantage of high imaging stability in the TEM mode. The interface is marked by a red dotted line. It is shown that the BTO film grown epitaxially on LSMO with high crystallinity. Atomic columns, including BaO, Ti, and O in BTO, as well as the (La,Sr)O, MnO_2 with clear MnO_6 wave-like oxygen octahedral tilting, are observed on a dark background. Figure 2b,c shows the magnification of the BTO area far and near the LSMO/BTO interface, marked by BTO-2 and BTO-1, respectively. The shift magnitude of Ti atoms relative to oxygen atoms in TiO_2 atomic columns along the [001] axis in BTO-1 is much larger than in BTO-2 as shown in Figure 2b,c, indicating a polarization enhancement at the interface. The shift of Ti atoms is downward, resulting in a downward-shifted positive charge center and polarization as illustrated in Figure 2d. In contrast, the sample with c-axis lattice parameter of 0.402 nm (sample grown at 570 °C and oxygen pressure of 12 Pa, which could be regarded as the reference sample), as well as another two samples (sample grown at 700 °C and sample grown at 570 °C and oxygen pressure of 9Pa) shows no obvious polarization enhancement at the interfacial area, as demonstrated in Figures S5 and S6, Supporting Information. It could be understood that the polarization is associated with the lattice parameter of c-axis and the tetragonality value (*c*/*a*). If there is no observed elongation of c-axis lattice parameter by XRD, there would be no polarization enhancement at the interface or the enhancement thickness is ultrathin (below the XRD detection limit, ≈two to three nanometers). Therefore, it could be seen that the polarization enhancement within few nanometers could be induced in the sample grown at 570 °C and low oxygen pressure (1Pa) by the above qualitative analysis.

© 2021 Wiley-VCH GmbH

2199160x, 2022, 2, Downloaded from https://onlinelibrary.wiley.com/doi/10.1002/aelm.202100876 by Peking University Health, Wiley Online Library on [04/09/2023]. See the Terms and Conditions (https://onlinelibrary.wiley.com/terms-and-conditions) on Wiley Online Library for rules of use; OA articles are governed by the applicable Creative Commons License

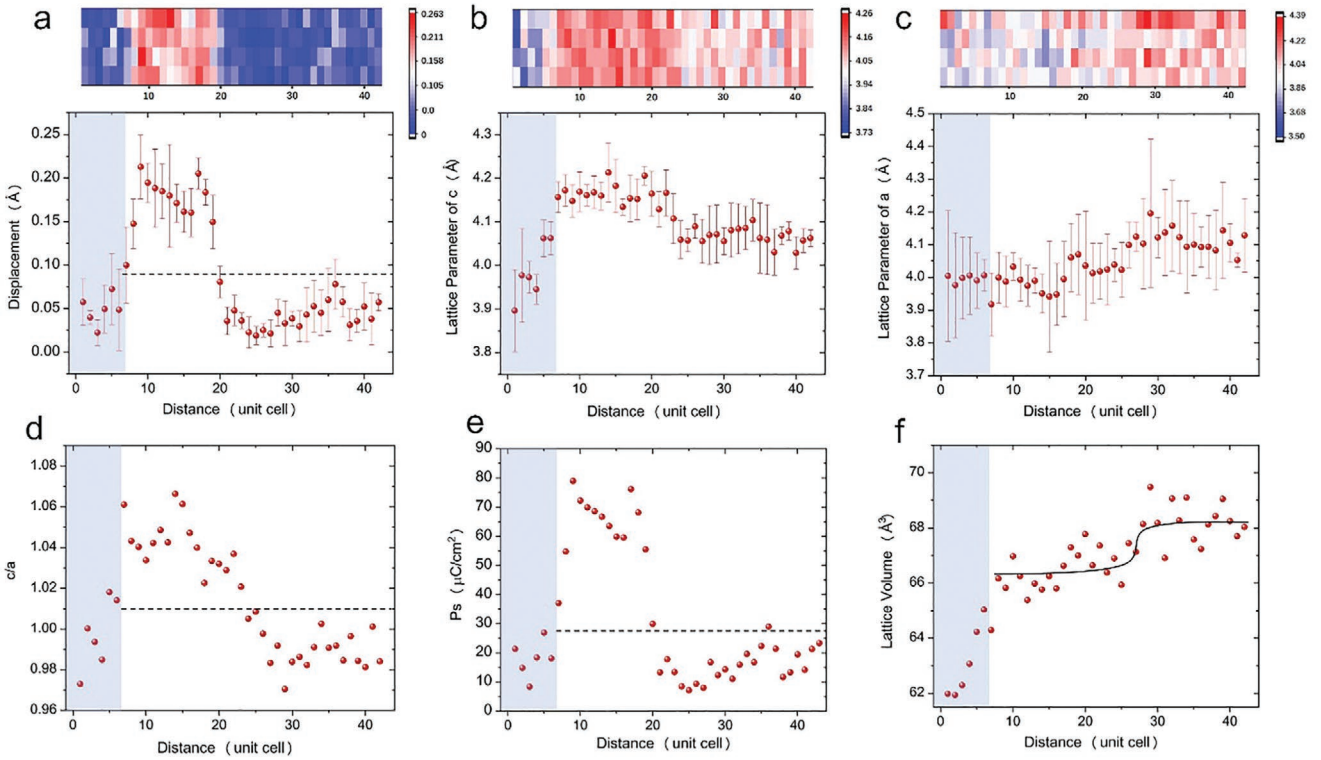

Figure 3. The quantitative analysis of the interfacial BTO films. The light blue regions on the left side of the profiles indicate the LSMO electrode. The spatial distribution (upper) and profiles (lower) of a) Ti displacement, b) lattice parameter of (c), and c) lattice parameter of (a). d) The tetragonality *c*/*a*, e) calculated spontaneous polarization, and f) lattice volume. The dashed lines in the figures indicate the responding values of the bulk BTO for comparison.

To quantitatively visualize the distribution of structural parameters including the polarization, the quantitative structural analysis based on the TEM image is conducted by mapping the positions of the atom columns, determined using a least-square fit by 2D Gaussian profile to each of the individual atomic intensity profiles.[23] The analyzed image is Figure 2a. All the measurements are based on the positions of the intensity maxima corresponding to the oxygen and Ti columns. The results including both spatial mapping at unit cell resolution and profiles of each row of structural parameters are shown in **Figure 3**. Figure 3a shows the profile of Ti displacements relative to oxygen atoms which reflects the magnitude of polarization. The obvious enhancement of Ti atoms displacement can be identified with a maximum of ≈20 pm within the thickness of 8 unit cells near the interface. This displacement value is more than two times larger than that of bulk BTO (≈7 pm). The displacement value dramatically reduces to nearly zero at the position more than 8 unit cells away from the interface. Figure 3b shows an analysis of the out-of-plane lattice spacing. The obvious elongation along the out-of-plane direction can be identified with a maximum of ≈0.42 nm within 8 unit cells from the interface in BTO, which then reduces to ≈0.403 nm. These two values are coincident with the aforementioned X-ray diffraction results where two out-of-plane diffraction peaks are observed in BTO. From Figure 3c, it can be seen that the in-plane lattice spacing keeps constant near the interface and then increases. An epitaxial strain gradient is demonstrated (from 0.39 to 0.415 nm). The gradient of strain could also be seen according to the geometric phase analysis (GPA) results. Based on the data shown above, the tetragonality *c*/*a* is derived with a maximum value of 1.062 within the thickness of 8 unit-cells near interface (highly tetragonal BTO) and a reduced value of ≈1.00 is shown in Figure 3d. The value is much larger than the bulk component and is close to the lead-based $PbTiO_3$ materials (see **Table 1**), which show excellent ferroelectric

Table 1. Comparisons of lattice parameters and tetragonalities of ferroelectric materials.

Materials	*a* [Å]	*c* [Å]	(*c*–*a*)/*a* [%]
BTO-1 (interfacial) phase in this work	3.94	4.18	6.2
BTO on $SrTiO_3$	3.96	4.11	3.7
BTO on $SrRuO_3/DyScO_3$	3.939	4.0989	4
BTO bulk	3.992	4.036	1.1
PTO bulk	3.899	4.15	6.44

© 2021 Wiley-VCH GmbH

2199160x, 2022, 2, Downloaded from https://onlinelibrary.wiley.com/doi/10.1002/aelm.202100876 by Peking University Health, Wiley Online Library on [04/09/2023]. See the Terms and Conditions (https://onlinelibrary.wiley.com/terms-and-conditions) on Wiley Online Library for rules of use; OA articles are governed by the applicable Creative Commons License

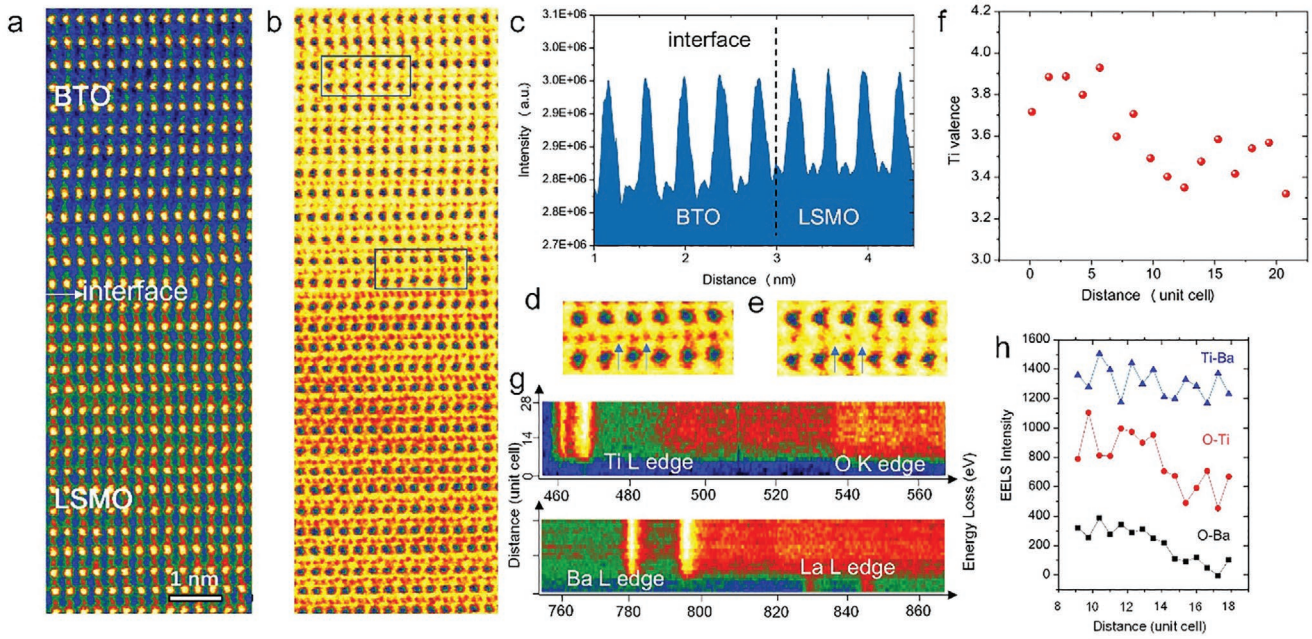

Figure 4. a,b) The atomic-scale HAADF-STEM and ABF-STEM images of BTO/LSMO heterostructures. c) The line profile of image intensity in HAADF-STEM, the interface is marked by the dashed line. The BTO near and relatively away from the interface marked by two squares in (b) are d,e) enlarged, the arrows pointing to the position of oxygen atoms. g) The EELS profiles across the BTO/LSMO interface. f) The Ti valence profile with the function of distance from the interface. h) The relative EELS intensities of Ti—Ba, O—Ti, and O—Ba, showing the oxygen content is relatively higher at the interface.

properties. The local spontaneous polarization along the out-of-plane direction is proportional to the displacement of Ti column from the center of the oxygen octahedron and the roughly estimated values are shown in Figure 3e. It verifies the dramatical polarization enhancement at the interface where a polarization as large as ≈70 μC cm^{-2} is revealed, which is much larger than that in bulk BTO (26μC cm^{-2}).[24,25] More importantly, the region with strongly enhanced polarization has a thickness of about 8 unit cells, which is much thicker than previous studies and would allow the application in practical functional devices,[9,10] such as ferroelectric tunnel junctions. Here, the P_S value is calculated based on the equation shown below:

$$P_S = \kappa\delta_{Ti} \quad (1)$$

where κ is a constant and δ_{Ti} is the displacement of Ti column from the center of oxygen octahedron.[26,27,28] Compared with the BTO films purely modulated by epitaxial strain on $SrTiO_3$ substrates, the polarization value in this work is much higher, indicating the existence of other tuning factors.[3] Figure 3f shows the profile of lattice volume based on the measurement of in-plane and out-of-plane lattice parameters. The measurement of lattice volume is a simple but effective way for the comparison of oxygen vacancies formation (the formation of oxygen vacancies usually results in the increase of lattice volume). Its value remains a low constant and gradually increases with the distance to the interface, suggesting the inhomogeneity of oxygen with an accumulation of oxygen vacancies at the relatively far region of the interfacial BTO and higher oxygen concentration near the interface. We note that the polarization enhanced area is located near the interface with a low concentration of oxygen vacancies, which is in contrast to the previous works using oxygen vacancies to elongate the lattices and enhance polarization.[9,10]

The chemical and electronic information are further investigated by atomic resolution STEM-EELS. From the atomic resolution high angle annular dark-field (HAADF)-STEM image in **Figure 4**a, the atomic flat chemical interface can be seen. As the image intensity is proportional to ≈Z$^{1.7}$(Z is the atomic number of atoms), the interface type can be determined as $BaO\text{-}MnO_2$ according to the intensity profiles at the interface shown in Figure 4c. To study the distribution of oxygen atoms, atomic resolution annular bright-field (ABF)-STEM is acquired and shown on the right side of Figure 4b. The darkest spots indicate La and Ba, whereas the weak contrast corresponds successively to Mn, Ti, and O. The local areas of BTO are magnified and shown in Figure 4d (region far from interface) and Figure 4e (region near interface). The oxygen signal is stronger at the interface, indicating a higher concentration of oxygen. Figure 4f is the EELS signals of Ti L edge, Ba L edge, and O K edge, recorded along the film growth direction. The chemical valence of Ti along film growth direction is extracted based on quantitative analysis of Ti $L_{2,3}$ edges, as shown in Figure 4f. The nominal valence is determined by linear fitting with Ti^{3+} and Ti^{4+} standard spectra obtained from reference compounds. It can be seen that the nominal valence of Ti is +3.9 near the interface and then reduces to +3.5 in the region relatively far from the interface. The oxygen ions carry a negative charge of –2, the Ba ion has a fixed valence of +2, therefore, the Ti valence may change due to the inhomogeneous distribution of oxygen to maintain the charge neutrality. It is possible that the area with higher Ti valence has a higher oxygen concentration. To evaluate the chemical content in the polarization enhanced sample, the EELS intensities of the elements (oxygen K edge, Ba L edge,

© 2021 Wiley-VCH GmbH

2199160x, 2022, 2, Downloaded from https://onlinelibrary.wiley.com/doi/10.1002/aelm.202100876 by Peking University Health, Wiley Online Library on [04/09/2023]. See the Terms and Conditions (https://onlinelibrary.wiley.com/terms-and-conditions) on Wiley Online Library for rules of use; OA articles are governed by the applicable Creative Commons License

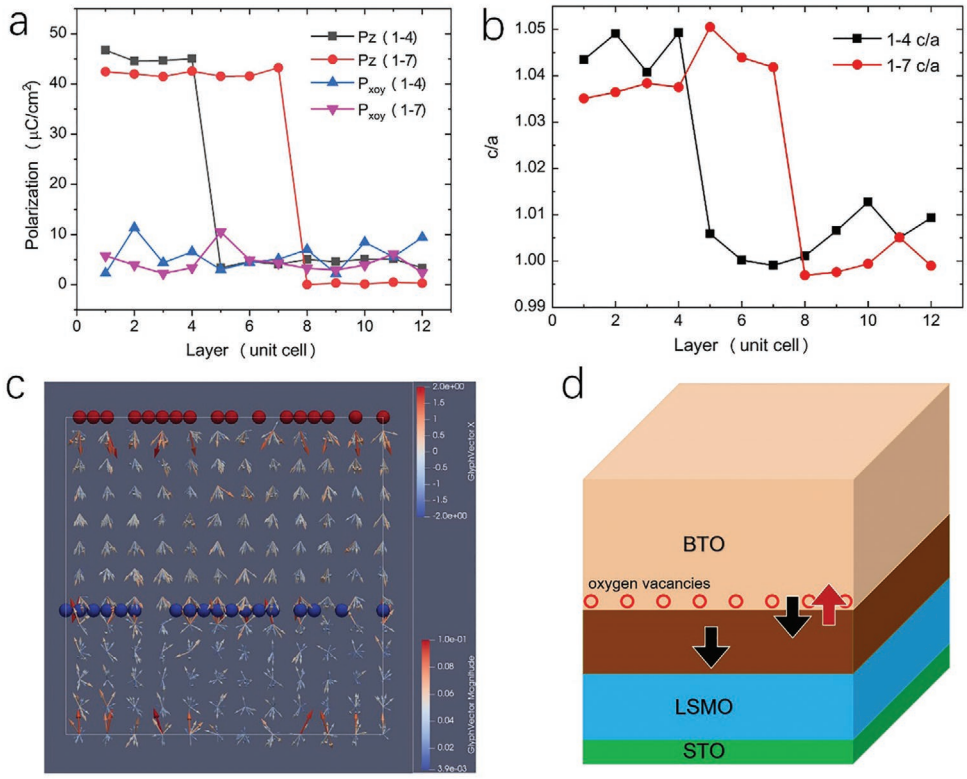

Figure 5. a,b) Shows the polarization and tetragonality in BTO calculated by first-principle MC simulation. c) The spatial distribution of polarization in the constructed lattices. d) Schematic configuration of oxygen vacancies-rich layer in BTO due to competition between interfacial charge induced polarization downwards (marked by dark arrow) and strain gradient induced polarization upwards due to flexoelectric effect (marked by red arrow). The induced electric field by polarization is opposite to the direction of polarization.

and Ti L edge) are also compared, as shown in Figure 4h. It is shown that the oxygen K edge intensity is relatively higher at the interface compared with the Ba L edge and Ti L edge.[29] which indicates a higher concentration of oxygen at the interfacial region. As a comparison, the Ti valence in the reference sample (grown at 570 °C and oxygen pressure of 12 Pa) is uniform (Ti+4) according to the EELS line scan results in Figure S8, Supporting Information, suggesting homogeneity of chemical content.

To further verify the mechanism of polarization enhancement near the interface due to oxygen inhomogeneity, we performed first-principles-based Monte–Carlo (MC) simulation.[26–31] For such simulation, the essential charge-dipole interaction has been added to the effective Hamiltonian and the MC simulation. Two separate charge layers in BTO lattices are used in our simulation to mimic the experimental situation. Focusing on the interface of LSMO/BTO, MnO_2-BaO stacking sequence induces a negative charge layer due to polar discontinuity. On the other hand, a certain number of oxygen vacancies are inserted at the upper region of BTO near the interface (the 4th and 7th layer from the interface). These two layers have the same number of charges ($2|e|$), ensuring electroneutrality in samples. The number of positive charges (oxygen vacancies) and interfacial negative charges is set as 30. **Figure 5**a shows the profile of polarization which suggests that the existence of charge can enhance the polarization of BTO to ≈45 μC cm^{-2} between these two charged layers. The axial ratio c/a is shown in Figure 5b, where a highly tetragonal BTO could form. The spatial distribution of polarization is shown in Figure 5c. The fluctuation data of medium BTO layers may be due to the inhomogeneous distribution of these charges, which are not real parallel charged metal plates. These results could support the experimentally observed polarization enhancement in the BTO layers. The polarization enhancement mechanism is explained as follows: The LSMO-BTO interface here is negatively charged (due to MnO_2-BaO polar interface) and the accumulation of oxygen vacancies above the interfacial BTO has positive charges. The induced electric field could push the Ti atoms with positive charges further downwards and the oxygen anion with negative charges upwards, resulting in enhanced polarization. In addition, the large strain gradient in BTO could induce a number of defects, meanwhile, there could be residual oxygen vacancies in the interfacial BTO lattices. Therefore, the expansion of the out-of-plane lattice parameter and enhancement of polarization could also possibly be partially contributed by the elastic- and electric-dipole moments of the defect dipoles in the interfacial BTO.

The mechanism for inhomogeneity distribution of oxygen can be explained as follows: The LSMO-BTO interface is negatively charged (due to the formation of MnO2-BaO type polar

© 2021 Wiley-VCH GmbH

2199160x, 2022, 2, Downloaded from https://onlinelibrary.wiley.com/doi/10.1002/aelm.202100876 by Peking University Health, Wiley Online Library on [04/09/2023]. See the Terms and Conditions (https://onlinelibrary.wiley.com/terms-and-conditions) on Wiley Online Library for rules of use; OA articles are governed by the applicable Creative Commons License

interface) inducing the polarization of BTO pointing downwards.[16] According to the polarization direction, the electric field inside the ferroelectric film is from interface to surface. Therefore, the oxygen vacancies with a positive charge inside BTO could be driven towards the surface direction. The accumulation of oxygen vacancies in the upper region could supply sufficient carrier density to eliminate the depolarization field and stabilize the highly tetragonal BTO phase. As the film thickness increases, the lattice compressive strain relaxes with the formation of structural defects. The strain gradient (relaxation of compressive strain) can induce a polarization pointing upwards (flexoelectric effect, as demonstrated in Figure S9, Supporting Information).[32] The competition (interfacial charge induced polarization downwards and flexoelectric effect induced polarization upwards) can reduce the magnitude of the internal electric field, polarization as well as the migration of oxygen vacancies, resulting in an oxygen vacancy-rich layer near the surface, as shown in Figure 5d.[6] Additionally, the strain relaxation with an accumulation of structural defects can induce larger lattice volume which can decrease the formation energy of oxygen vacancies and promote their formation. Normally, the thickness to maintain elastic energy (highly tetragonal BTO phase assistant by oxygen vacancies in this situation) could last for several nanometers. Therefore, the enhanced polarization could extend longer than the literature research via oxygen inhomogeneity due to differences in mechanisms.[9,10]

According to the recent report, BTO could be used as a super-elastic ferroelectric membrane with large polarization,[33] therefore, our finding could be applied to tune the properties of free-standing ferroelectric films which could be used for flexible electronic devices. It is also should be noted that polarization enhancement could be achieved by introducing secondary phases and using the interphase strain to elongate the c-axis lattice parameter of ferroelectric films, such as PbO in $PbTiO_3$ system.[34] The manipulation of oxygen inhomogeneity could be combined with interphase engineering for the further tuning of electronic properties and ferroelectric and ferromagnetic properties in oxide nanostructures.[35,36]

3. Conclusion

In summary, we have explored the effect of oxygen inhomogeneity on the structure and polarization in ferroelectric BTO films on STO substrates. The inhomogeneous distribution of oxygen along c-axis was achieved by systematically tuning the growth temperature and oxygen pressure, which modulate the flexoelectricity and therefore the internal electric field. In this work, enhanced tetragonality and polarization as high as 70 μC cm^{-2} were reached. We note that the interfacial oxygen vacancies have shown the capability of polarization enhancement in early works, the polarization enhanced area is oxygen-deficient, the mechanism is usually based on interfacial charge discontinuity induced formation of oxygen vacancies with lattice expansion, the thickness of polarization enhanced area is limited to ≈1–2 unit cells. Our work uses the growth conditions to modulate the internal electric field which is the driving force of oxygen migration during growth to achieve oxygen inhomogeneity. The cooperation of interfacial charge and the positively charged oxygen vacancies in the adjacent layer could form an electric field and lead to polarization enhancement. This area has a low concentration of oxygen vacancies and has a thickness of ≈8 unit cells. This work provides a new application of utilizing oxygen to engineer the ferroelectrics and paves the way for the development of practical nanoscale ferroelectric devices.

4. Experimental Section

Thin Film Preparation: Stoichiometric BTO and LSMO targets were prepared by a conventional ceramic sintering method. STO (001) substrates were first etched by buffered hydrofluoric acid and then thermally annealed to obtain an atomic flat TiO_2 termination. The LSMO layer was deposited by ablating the ceramic target using a KrF excimer laser (wavelength of 248 nm, Lambda Physik) and a repetition rate of 2 Hz with a substrate temperature of 750 °C. The laser energy density on the target was 2 J cm^{-2}. BTO films were deposited by ablating the ceramic target at a repetition rate of 3 Hz. During the deposition of BTO, the substrate temperature was controlled to be 570, 700, and 730 °C. The oxygen pressures (1, 9, and 12 Pa) were used to modify the oxygen content.

Structural Analysis: X-ray diffraction analysis was performed by a Rigaku Smartlab diffractometer. Cross-sectional TEM samples were prepared using conventional mechanical grinding and polishing. The final thinning by Ar-ion milling was carried out in a Gatan PIPS II milling machine with a liquid nitrogen-cooled stage. The high-resolution TEM was performed on a Thermal Fisher Titan 80–300 microscope with a spherical aberration corrector for the objective lens. The spherical aberration Cs was adjusted to −13.6 μm. JEOL ARM200F with spherical aberration corrector for condenser lens was used for the STEM and EELS characterization.

Theoretical Analysis: The first-principles-based effective Hamiltonian for BTO used here has been developed.[26,30] A new energy item was introduced into total energy to account for the charge-dipole interaction. The new energy expression is given by:

$$E^{\text{tot}}. = E^{\text{self}}\left(\{\boldsymbol{u}\}\right) + E^{\text{dpl}}\left(\{\boldsymbol{u}\}\right) + E^{\text{short}}\left(\{\boldsymbol{u}\}\right). + E^{\text{elas}}\left(\{\eta_l\},\{\eta_H\}\right) + E^{\text{int}}\left(\{\boldsymbol{u}\},\{\eta_l\},\{\eta_H\}\right). + E^{\text{chg-dpl}}\left(\{\boldsymbol{u}\},q\right). \quad (2)$$

Here $E^{\text{self}}(\{\boldsymbol{u}\})$, $E^{\text{dpl}}(\{\boldsymbol{u}\})$, $E^{\text{short}}(\{\boldsymbol{u}\})$, $E^{\text{elas}}(\{\eta_l\},\{\eta_H\})$, $E^{\text{int}}(\{\boldsymbol{u}\},\{\eta_l\},\{\eta_H\})$, and $E^{\text{chg-dpl}}(\{\boldsymbol{u}\}, q)$, are all the local-mode self-energy, long-range dipole-dipole interactions, short-range interactions between soft modes, elastic energy, interactions between the local modes and local strain, and long-range charge-dipole interactions energy, respectively. u is the local soft-mode amplitude vector (directly proportional to the local polarization), q is the charges induced by the aliovalent doping ions, boundary charges, free charges, or cations/anions vacancies, and η_H (η_l) is the six-component homogeneous (inhomogeneous) strain tensor in Voigt notation. The charge-dipole energy was treated with the Ewald method and the details can be found.[31]

Based on the above effective Hamiltonian, MC simulations were performed with a pseudo-cubic supercell of size 12 × 12 × 12 (i.e., 1728 unit cells) with periodic boundary conditions. The charges were randomly distributed on their fixed layer. For simplicity, the charges were supposed that oxygen vacancies in BTO and charges in LSMO with the value of charges of $q = 2\,|e|$. For each of the doped samples, the system was gradually cooled down from high temperature (≈550 K) to room temperature (≈300 K) with a step of 10 K and used 320 000 MC sweeps.

Supporting Information

Supporting Information is available from the Wiley Online Library or from the author.

© 2021 Wiley-VCH GmbH

2199160x, 2022, 2, Downloaded from https://onlinelibrary.wiley.com/doi/10.1002/aelm.202100876 by Peking University Health, Wiley Online Library on [04/09/2023]. See the Terms and Conditions (https://onlinelibrary.wiley.com/terms-and-conditions) on Wiley Online Library for rules of use; OA articles are governed by the applicable Creative Commons License

Acknowledgements

This work was financially supported by the National Key Research and Development Program of China (Grant No. 2019YFB2005801, 2016YFA0300804), the National Natural Science Foundation of China (Grants No. 51731003, No. 51971023, No. 51927802, No. 11974023, No. 11974268, No. 52061135205), and the Fundamental Research Funds for the Central Universities (FRF-MP-20-27).

Conflict of Interest

The authors declare no conflict of interest.

Data Availability Statement

The data that supports the findings of this study are available in the supplementary material of this article.

Keywords

ferroelectrics, flexoelectricity, internal electric field, oxygen vacancies, polarization

Received: August 18, 2021
Revised: September 26, 2021
Published online: October 20, 2021

[1] S. Das, Y. L. Tang, Z. Hong, M. A. P. Gonçalves, M. R. McCarter, C. Klewe, K. X. Nguyen, F. Gómez-Ortiz, P. Shafer, E. Arenholz, V. A. Stoica, S.-L. Hsu, B. Wang, C. Ophus, J. F. Liu, C. T. Nelson, S. Saremi, B. Prasad, A. B. Mei, D. G. Schlom, J. Íñiguez, P. García-Fernández, D. A. Muller, L. Q. Chen, J. Junquera, L. W. Martin, R. Ramesh, *Nature* **2019**, *568*, 368.
[2] N. A. Spaldin, R. Ramesh, *Nat. Mater.* **2019**, *18*, 203.
[3] D. G. Schlom, L. Q. Chen, C. B. Eom, K. M. Rabe, S. K. Streiffer, J. M. Triscone, *Annu. Rev. Mater. Res.* **2007**, *37*, 589.
[4] M. E. Lines, A. M. Glass, G. Burns, *Phys. Today* **1978**, *31*, 56.
[5] D. Damjanovic, *Rep. Prog. Phys.* **1998**, *61*, 1267.
[6] D. Lee, B. C. Jeon, S. H. Baek, S. M. Yang, Y. J. Shin, T. H. Kim, Y. S. Kim, J.-G. Yoon, C. B. Eom, T. W. Noh, *Adv. Mater.* **2012**, *24*, 6490.
[7] A. R. Damodaran, E. Breckenfeld, Z. Chen, S. Lee, L. W. Martin, *Adv. Mater.* **2014**, *26*, 6341.
[8] Y.-M. Kim, A. Morozovska, E. Eliseev, M. P. Oxley, R. Mishra, S. M. Selbach, T. Grande, S. T. Pantelides, S. V. Kalinin, A. Y. Borisevich, *Nat. Mater.* **2014**, *13*, 1019.
[9] Y. Liu, Y. L. Zhu, Y.-L. Tang, Y.-J. Wang, Y.-X. Jiang, Y.-B. Xu, B. Zhang, X.-L. Ma, *Nano Lett.* **2017**, *17*, 3619.
[10] Q. Qiao, Y. Zhang, R. Contreras-Guerrero, R. Droopad, S. T. Pantelides, S. J. Pennycook, S. Ogut, R. F. Klie, *Appl. Phys. Lett.* **2015**, *107*, 201604.
[11] Z. Wen, C. Li, D. Wu, A. Li, N. Ming, *Nat. Mater.* **2013**, *12*, 617.
[12] X. B. Ren, *Nat. Mater.* **2004**, *3*, 91.
[13] D. Lee, B. C. Jeon, A. Yoon, Y. J. Shin, M. H. Lee, S. D. Song, M. Kim, J. S. Chung, J. G. Yoon, *Adv. Mater.* **2014**, *26*, 5005.
[14] M. F. Chisholm, W. Luo, M. P. Oxley, S. T. Pantelides, H. N. Lee, *Phys. Rev. Lett.* **2010**, *105*, 197602.
[15] K. Kathan-Galipeau, P. Wu, Y. Li, L.-Q. Chen, A. Soukiassian, X. Xi, D. G. Schlom, D. A. Bonnell, *ACS Nano* **2011**, *5*, 640.
[16] P. Yu, W. Luo, D. Yi, J. X. Zhang, M. D. Rossell, C.-H. Yang, L. You, G. Singh-Bhalla, S. Y. Yang, Q. He, Q. M. Ramasse, R. Erni, L. W. Martin, Y. H. Chu, S. T. Pantelides, S. J. Pennycook, R. Ramesh, *Proc. Natl. Acad. Sci. U. S. A.* **2012**, *109*, 9710.
[17] A. Ohtomo, H. Y. Hwang, *Nature* **2004**, *427*, 423.
[18] B. Wang, Y. Gu, S. Zhang, L.-Q. Chen, *Prog. Mater. Sci.* **2019**, *106*, 100570.
[19] G. Catalan, A. Lubk, A. H. G. Vlooswijk, E. Snoeck, C. Magen, A. Janssens, G. Rispens, G. Rijnders, D. H. A. Blank, B. Noheda, *Nat. Mater.* **2011**, *10*, 963.
[20] P. Zubko, G. Catalan, A. K. Tagantsev, *Annu. Rev. Mater. Res.* **2013**, *43*, 387.
[21] D. Lee, A. Yoon, S. Y. Jang, J. G. Yoon, J. S. Chung, M. Kim, *Phys. Rev. Lett.* **2011**, *107*, 57602.
[22] C. L. Jia, M. Lentzen, K. Urban, *Science* **2003**, *299*, 870.
[23] L. Houben, A. Thust, K. Urban, *Ultramicroscopy* **2006**, *106*, 200.
[24] J. P. Gordon, H. J. Zeiger, C. H. Townes, *Phys. Rev.* **1955**, *99*, 1264.
[25] J. J. Wang, F. Y. Meng, X. Q. Ma, M. X. Xu, L. Q. Chen, *J. Appl. Phys.* **2010**, *108*, 064101.
[26] W. Zhong, D. Vanderbilt, K. M. Rabe, *Phys. Rev. B* **1995**, *52*, 6301.
[27] C. L. Jia, S. B. Mi, K. Urban, I. Vrejoiu, M. Alexe, D. Hesse, *Phys. Rev. Lett.* **2009**, *102*, 117601.
[28] A. Janotti, C. G. V. D. Walle, *Nat. Mater.* **2007**, *6*, 44.
[29] Z. Li, B. Michel, Y. Zhen, P. Ren, L. Wang, L. Cao, X. Yu, C. Ke, M. B. H. Breese, A. Rusydi, W. Zhu, Z. Dong, Y. L. Foo, *Adv. Funct. Mater.* **2012**, *22*, 4312.
[30] T. Nishimatsu, M. Iwamoto, Y. Kawazoe, U. V. Waghmare, *Phys. Rev. B* **2010**, *82*, 134106.
[31] D. Wang, J. Liu, J. Zhang, S. Raza, X. Chen, C. L. Jia, *Comput. Mater. Sci.* **2019**, *162*, 314.
[32] T. Xu, J. Wang, T. Shimada, T. Kitamura, *J. Phys.: Condens. Matter* **2013**, *25*, 415901.
[33] G. Dong, S. Li, M. Yao, Z. Zhou, Y.-Q. Zhang, X. Han, Z. Luo, J. Yao, B. Peng, Z. Hu, H. Huang, T. Jia, J. Li, W. Ren, Z.-G. Ye, X. Ding, J. Sun, C.-W. Nan, L.-Q. Chen, J. Li, M. Liu, *Science* **2019**, *366*, 475.
[34] L. Zhang, J. Chen, L. Fan, S. Diéguez, J. Cao, Z. Pan, Y. Wang, J. Wang, M. Kim, S. Deng, J. Wang, H. Wang, J. Deng, R. Yu, J. F. Scott, X. Xing, *Science* **2018**, *361*, 494.
[35] T.-C. Su, J. Zhang, W. Zhang, *Rare Met.* **2021**, *40*, 1858.
[36] X. R. Zhou, Z. X. Feng, P. X. Qin, H. Yan, S. Hu, H. X. Guo, X. N. Wang, H. J. Wu, X. Zhang, H. Y. Chen, X. Qiu, *Rare Met.* **2020**, *39*, 368.

© 2021 Wiley-VCH GmbH

2199160x, 2022, 2, Downloaded from https://onlinelibrary.wiley.com/doi/10.1002/aelm.202100876 by Peking University Health, Wiley Online Library on [04/09/2023]. See the Terms and Conditions (https://onlinelibrary.wiley.com/terms-and-conditions) on Wiley Online Library for rules of use; OA articles are governed by the applicable Creative Commons License